eman ta zabal zazu
Universidad del País Vasco
Euskal Herriko Unibertsitatea

ZTF-FCT
Zientzia eta Teknologia Fakultatea
Facultad de Ciencia y Tecnología
Euskadi 2006

Bachelor Thesis
Degree in Physics

Detection of particles with a cloud chamber

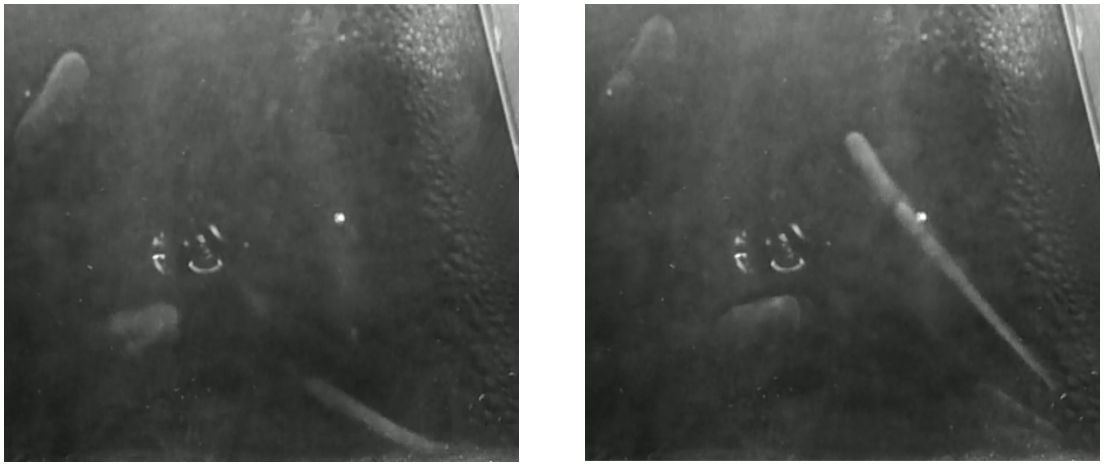

Snapshots of a cosmic ray shower recorded in the project.

Author:
Iván Esteban Muñoz
Directors:
Gunar Schnell
Charlotte Van Hulse

Leioa, 24th June 2015

"The most original and wonderful instrument in scientific history"

—Ernest Rutherford

"The final court of appeal in physics"

Abstract

Cloud chambers were essential devices in early nuclear and particle physics research. Superseded by more modern detectors in actual research, they still remain very interesting pedagogical apparatus.

This thesis attempts to give a global view on this topic. To do so, a review of the physical foundations of the diffusion cloud chamber, in which an alcohol is supersaturated by cooling it with a thermal reservoir, is carried out. Its main results are then applied to analyse the working conditions inside the chamber. The analysis remarks the importance of using an appropriate alcohol, such as isopropanol, as well as a strong cooling system, which for isopropanol needs to reach $\lesssim -40°\mathrm{C}$.

That theoretical study is complemented with experimental tests that were performed with what is the usual design of a home-made cloud chamber. An effective setup is established, which highlights details such as a grazing illumination, a direct contact with the cooling reservoir through a wide metal plate, or the importance of avoiding vapour removal. Apart from that, video results of different phenomena that cloud chamber allow to observe are also presented.

Overall, it is aimed to present a physical insight that pedagogical papers usually lack.

Contents

Chapter 1

Introduction and purpose

Cloud chambers are one of the most simple instruments to study elementary particles. The fundamental principle behind them is *the supersaturation of a gaseous substance*, a state in which the air, or any other gas, contains more vapour of that substance than it can hold in a stable equilibrium. The passage of ionising particles then creates a track of ions, which under supersaturation conditions act as condensation nuclei. The condensation of the vapour on these nuclei allows an easy identification of the trajectories of the particles, leading to a straightforward study of their properties.

This idea has undergone different designs and uses, being nowadays eclipsed by more modern detection devices. Throughout the years, it has evolved from being an essential research tool to remaining only as a pedagogical device. To better understand this process, probably the best approach is a brief historical outline.

1.1 Historical overview

Cloud chambers were first studied in the Cavendish Laboratory of Cambridge by C.T.R. Wilson in 1911 [1] as, initially, part of his research on condensation nuclei and cloud formation. The required supersaturation, which only lasted for a few seconds, was reached by periodically cooling air below the condensation point of water with repeated adiabatic expansions. Wilson's original design can be seen in Figure 1.1.

That design had the problem of being intermittent; therefore, ions from particles that passed between expansions diffused before having vapour condensed on them, leading to a great amount of diffuse tracks. In order to avoid this problem, Wilson applied an electric field that swept those ions out of the working area.

It was soon realised that all ionising radiation known back then[1] could be studied with this device. Because of this, Wilson received the 1927 Nobel Prize in Physics. Even though his "expansion" cloud chamber could only maintain the supersaturation for a few seconds, fundamental breakthroughs in the field of particle physics were made with it. To mention some significant examples, Wilson himself confirmed the Compton effect discovering the Compton recoil electrons in 1923 [2]. The first antiparticle, the positron, the first second-generation particle, the muon, and the first strange particle, the kaon, were also first identified using this device [3–5]. As an example, Figure 1.2 shows the photograph of the track that, because of its deflection in an external magnetic field, first led to the identification of the positron.

[1] Ionising electromagnetic radiation can be studied via the electrons it ejects.

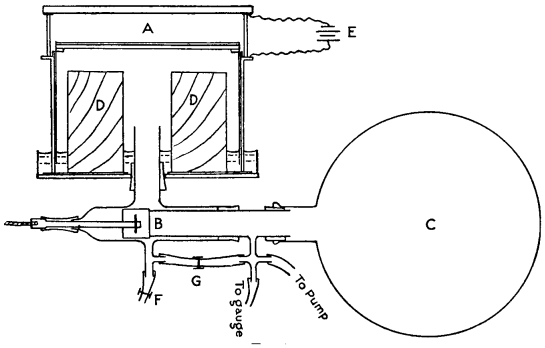

Figure 1.1: Wilson's original design, based on adiabatic expansions. The working mechanism is based on a piston, B, that periodically puts the chamber, A, in contact either with a vacuum bulb, C, or with the atmosphere, F, thus causing periodic adiabatic expansions. The setup for the creation of the sweeping electric field, E, can also be seen.

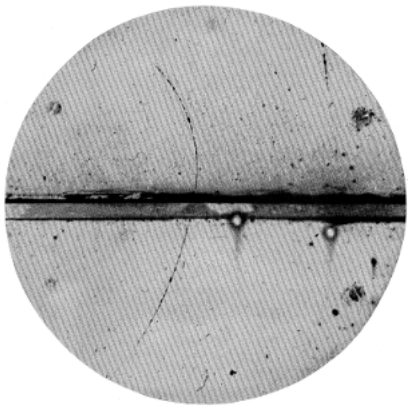

Figure 1.2: A positron passing through a lead plate. The curvature difference between both sides of the plate helped to determine its direction of motion and, consequently, the sign of its charge. As will be developed in Section 2.2, its energy and range in air made clear that it was not a proton.

Although in 1933 Wilson improved the design with an easier to-make cloud chamber whose cooling mechanism was an adiabatic pressure drop [6], it still suffered from being intrinsically intermittent. This problem was partly overcome by using Geiger counters placed above and below the chamber to trigger its activation when a particle was known to have passed.

Trying to fix that issue some designs of continuous cloud chambers were published [7, 8]. However, they weren't stable enough to photographically record tracks of particles. Because of that, in 1938 A. Langsdorf, in his Ph.D. thesis, presented what he called a *continuously sensitive diffusion cloud chamber* [9].

His design can be seen in Figure 1.3. Heated vapour diffused through another gas from the top part of a chamber until it reached the floor, an area cooled below the condensation temperature of the vapour. Therefore, a layer of supersaturated vapour was continuously maintained, allowing an easy recording of tracks.

He also added a grid of wires to apply an electric field with the aim, as in expansion cloud chambers, of getting rid of the ions formed in the upper part. These ions would otherwise diffuse

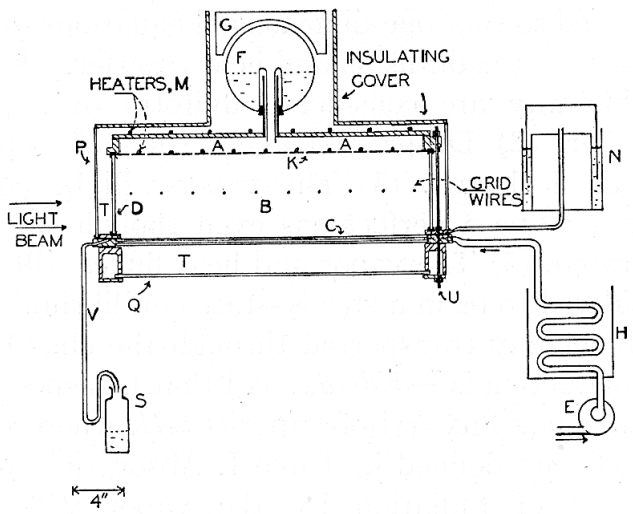

Figure 1.3: Langsdorf's original design. S, N, and H are the condensed vapour, gas and cooling liquid reservoirs, respectively. The liquid was cooled with dry ice, that is, CO_2 in its solid state.

downwards, causing condensation and a permanent unwanted "rain". Other scientists, on the other hand, suggested using this electric field to sweep ions towards the supersaturated area [10], increasing the amount of condensation events; therefore preventing a spontaneous fog formation that would decrease the quality of the tracks. Anyhow, its different effects show that unlike expansion cloud chambers, continuously sensitive cloud chambers did not necessarily require an electric field.

This chamber had significant advantages of stability and building simpleness over the expansion ones. It had, though, various drawbacks, among which Langsdorf highlighted the following:

1. It required the working area to be horizontal, an inconvenience for the study of cosmic rays, which mostly hit vertically [11].

2. The large horizontal dimensions of the chamber complicated the application of strong and uniform magnetic fields for track deflection.

3. The limited supply of vapour made the use of strong ionization sources difficult.

4. Because of the continuous supersaturation, any radioactive source placed inside the chamber would constantly have vapour condensed on it; therefore reducing the quality of the supersaturated state.

It was, though, clearly superior to the expansion cloud chamber for the study of condensation, due to the continuous maintenance of a supersaturated state. Nowadays more sophisticated designs are still used in that area of science (see, for instance, Ref. [12]).

Because of its problems, however, only in the early 1950s diffusion cloud chambers began to be used in nuclear physics research [13]. Moreover, major research to solve the remaining problems of diffusion cloud chambers stopped when in 1952 D.A. Glaser invented the bubble chamber [14], instantly replacing cloud chambers. Bubble chambers used an overheated liquid instead of a supersaturated gas for track formation, therefore giving more stability and allowing easy resets and triggering that reduced the background signal. These chambers were later superseded by wire

chambers, which electronically detect the ionisation caused by travelling particles and allow a more systematic data acquisition.

Nevertheless, diffusion cloud chambers still remained interesting pedagogically, being easy to build and carry. Because of that, they are prominent devices in nuclear and particle physics demonstrations.

1.2 The diffusion cloud chamber as a pedagogical device

Although diffusion cloud chambers were never broadly used in nuclear and particle physics research, being easy to build an carry they still remain interesting educational instruments. Nowadays, they are an easy way of learning about and visualising elementary particles and radiation as well as condensation and cloud formation.

In order to improve even more the simpleness of the chamber, an idea first proposed by T.S. Needels and C.E. Nielsen [10] is usually used. This design, which can be seen in Figure 1.4, consists of a glass container sitting on a surface in direct contact with dry ice and of an alcohol reservoir, which originally was just a wet cardboard, on top of the container at room temperature. Therefore, it easily attains the desired conditions, a temperature gradient and alcohol diffusing from the hot to the cold part.

This provides an easy way of visualizing a whole variety of phenomena, from cosmic rays to radioactivity or particle scattering. It also gives an interesting insight into the physics of condensation and cloud formation. The purpose of this thesis will be to analyse these processes, trying to explain *how* and *under which conditions* a home-made diffusion cloud chamber optimally shows tracks as well as *what* can be observed. Additionally, a report and results of a diffusion cloud chamber that was built in the Theoretical Physics and History of Science Department will be provided, allowing to directly test what *can* and *cannot* be done with home-made diffusion cloud chambers.

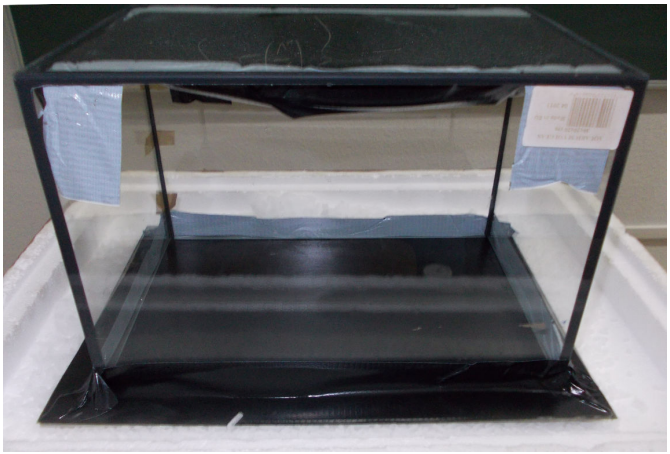

Figure 1.4: Usual design of a home-made cloud chamber. The chamber in the image is the one that was built as part of this thesis.

Chapter 2

Physics Insight. Condensation

Condensation phenomena play a fundamental role in cloud chambers. The study of these processes gives an insight into the physical principles that make them work, thus enabling a determination of the most appropriate experimental conditions. What is more, diffusion cloud chambers are highly useful devices for the study of condensation and cloud formation, an area of science that is still active nowadays.

Throughout this chapter, a review of the main theories on condensation will be carried out. Their most important results will be applied to quantitatively study a diffusion cloud chamber of isopropanol diffusing into air with its bottom surface cooled with dry ice.

Unless otherwise specified, the necessary properties of substances will be extracted from *The CRC Handbook of Chemistry and Physics, 90th Edition* [15], *The Handbook of Physical-Chemical Properties and Environmental Fate for Organic Chemicals* [16], and *Transport Properties of Chemicals and Hydrocarbons* [17].

2.1 Physics of liquid drop formation

An essential topic that needs to be tackled in a rigorous treatment of condensation is *the conditions under which drops are formed*. Its study leads to a better understanding of track formation in cloud chambers.

2.1.1 The Ostwald-Freundlich equation

The formation of drops is not as straightforward as having a gas in its saturated state. In fact, as it was first shown by Lord Kelvin [18] and Robert von Helmholtz [19], due to surface tension, the saturation vapour pressure over a drop of radius r, p_r, is higher than the saturation vapour pressure over a plane surface, p_∞[1], by an amount given by

$$p_r = p_\infty \exp\left(\frac{2\gamma}{r}\frac{M}{RT\rho}\right), \tag{2.1}$$

where γ is the surface tension, ρ is the density of the liquid to be formed, M is its molar mass, R is the gas constant and T is the temperature. This equation is known as the Ostwald–Freundlich equation. Given the importance of the dimensionless quantity $\frac{p}{p_\infty}$, it is common to refer to it as the *supersaturation*, S.

[1] This last quantity is what is commonly called vapour pressure.

That equation has the consequence that for $S \leq 1$ droplets are unstable: being the exponent always positive, they require on their surface a much higher pressure than the saturation pressure p_∞. *Unless the vapour is in a supersaturated state* where $p > p_\infty$, $p = p_r$ will never be reached and any droplet will boil and completely evaporate. What is more, the Ostwald-Freundlich equation shows that *drops can not be spontaneously created*, requiring for an infinitesimally small droplet an exponentially high supersaturation.

If, however, somehow a drop of a big enough radius is formed, the required supersaturation could be attainable and the drop may be stable. Furthermore, when the vapour starts condensing on the drop, its radius increases, the required pressure for condensation p_r falls and the drop continues growing, finally reaching a visible size. Here *condensation nuclei* are thus naturally introduced as small particles of finite radius that allow, by condensation on them, the beginning of this process.

This behaviour can also be understood graphically. In Figure 2.1 the supersaturation $S_r = p_r/p_\infty$ is plotted as a function of r for different temperatures[2]. 194.75 K corresponds to the temperature of dry ice.

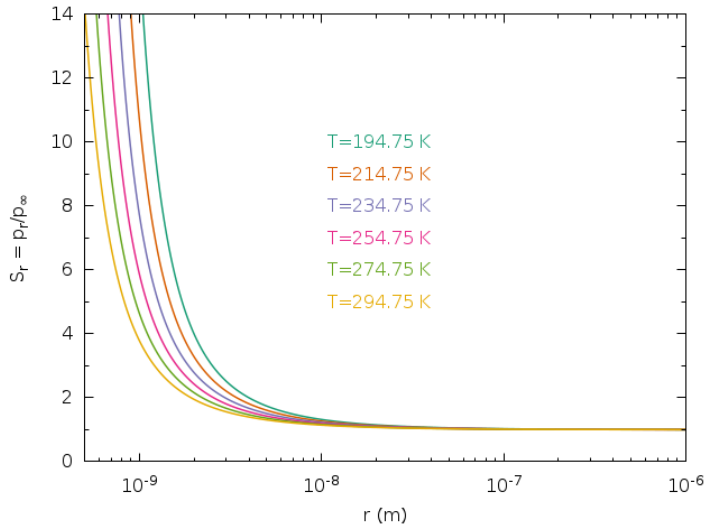

Figure 2.1: Vapour pressure for simple drops. Data of isopropanol is used.

As can be seen there, the vapour pressure on the surface of a drop is a decreasing function of its radius. As a consequence, once the required supersaturation for a certain drop radius is attained, nuclei of that radius will start to grow drops on them, increasing their radius and thus decreasing the pressure needed for the drops to be stable. That way, the growth will indefinitely continue and the droplet will reach a visible size.

It is as well seen that the required supersaturation for the formation of a drop with a fixed radius increases when the temperature is decreased.

Finally, since in equation (2.1) S_r grows exponentially, it is easy to get an estimation of the radius for which p_r is not ridiculously higher than p_∞, that is, the order of magnitude of the minimum radius of condensation nuclei. For isopropanol at $T = 194.75$ K, $p_r \sim p_\infty$ for $r \sim 10^{-9}$m, which gives an idea of the length scale involved in drop formation.

[2]For a copy of the thesis with, according to Ref. [20], colour-blind friendly plots, see the file `Colour_blind.pdf`. Most of the colour palettes used there should also be photocopy-friendly.

2.1.2 Condensation on charged nuclei

J.J. Thomson showed [21] that if a drop has a charge of value e, which is the case in cloud chambers since drops are formed around ions, equation (2.1) must be modified to

$$p_r = p_\infty \exp\left[\frac{M}{RT\rho}\left(\frac{2\gamma}{r} - \frac{e^2}{32\pi^2\varepsilon r^4}\right)\right], \tag{2.2}$$

where ε is the dielectric constant of the surrounding medium.

In this case the stability analysis is not as straightforward as with the Ostwald-Freundlich equation and is better understood graphically. Figure 2.2 represents the supersaturation at the surface of a stable charged drop, S_r, as a function of its radius, r.

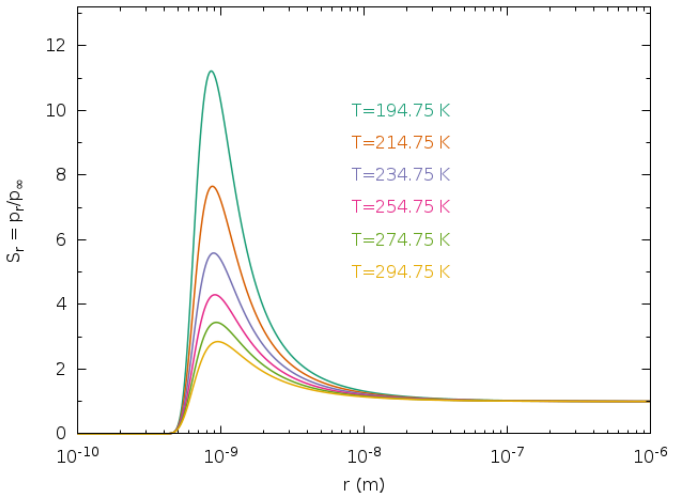

Figure 2.2: Vapour pressure for charged drops. Data of isopropanol is used. $\varepsilon = \varepsilon_0$ is taken for the surrounding gas, as is common for gases.

The most notable aspect of Figure 2.2 is that there is a region where S_r is an increasing function of r. Therefore, in that region droplets will *not* spontaneously grow until becoming visible: if their radius begins to increase, they require more supersaturation to continue growing.

There are, however, two remarkable phenomena. Firstly, for charged nuclei infinitesimally small droplets *can* be formed. What is more, for each supersaturation S up to a certain limit there are two critical radii $r_c(S)$ for which $p_{r_c}/p_\infty = S$. If $r_{\text{c min}}$ is the smallest of the critical radii, given a supersaturation S *any* charged drop of radius $r \leq r_{\text{c min}}(S)$ will spontaneously grow until reaching a stable size $r_{\text{c min}}$. Similarly, if $r_{\text{c max}}$ is the large critical radius, *any* charged drop of radius $r \geq r_{\text{c max}}(S)$ will spontaneously become larger until it reaches a visible size. It is immediate to show from equation (2.2) that the critical radii fulfil the following condition:

$$\frac{\rho RT}{M}\ln S = \frac{2\gamma}{r_c} - \frac{e^2}{32\pi^2\epsilon r_c^4} \tag{2.3}$$

which for isopropanol, taking $\varepsilon = \varepsilon_0$ for the surrounding gas, gives $r_c \sim 5\,\text{Å}$ for $S \sim 1$. Since it is inevitable to have some ions in the air, droplets of such size will always be present in any supersaturated state. Those droplets, however, will not grow and reach a visible size.

Nevertheless, charged drops have another remarkable property: if the supersaturation is high enough, the radius $r_{\mathrm{c\ min}}$ of the spontaneously formed droplets could reach the maximum of Figure 2.2 and get to the descending part of the graph. There, it would automatically grow becoming, in the end, visible. In other words, for a supersaturation higher than the maximum of Figure 2.2, *every single charged particle in the medium will be an effective condensation nucleus*. As a consequence, *every ionising particle that transverses the chamber generating a sufficient amount of ions will leave a visible track*.

This "critical" supersaturation S_c, in principle the minimum required in cloud chambers for optimum performance, is given by

$$S_c = \exp\left[\frac{3M}{2RT\rho}\gamma^{4/3}\left(\frac{16\pi^2\epsilon}{e^2}\right)^{1/3}\right], \tag{2.4}$$

which, for isopropanol at $T = 194.75$ K, is $S_c = 10.1$. According to Ref. [22], the existence of a critical supersaturation was observed by C.T.R. Wilson when he performed his first tests with cloud chambers.

Lastly, it is interesting to point out that this model also shows that higher supersaturations are required for drop formation at low temperatures.

2.1.3 More sophisticated models

Both the Ostwald-Freundlich equation, (2.1), and its analogue for charged nuclei, equation (2.2), were developed under several assumptions that, when relaxed, give rise to different $S_r(r)$ curves [22].

For instance, when it is considered that charged drops might electrify the surrounding gas different condensation center efficiencies are found for negative and positive ions depending on the supersaturated vapour being used.

Nevertheless, the most important single improvement of the model is probably the consideration that the surface tension may depend on the radius. This idea, which has good theoretical and experimental support [23, 24], adds a term $\frac{M}{RT\rho}\frac{d\gamma}{dr}$ to equations (2.1) and (2.2), and leads to the conclusion that the $S_r(r)$ curve has a shape similar to the one in Figure 2.3.

Under this assumption, for the same reason as in Figure 2.2, there are always droplets for every supersaturation degree. However, until S is high enough for them to reach the point A, or A' if they are charged, these droplets will not grow up to a visible size. As soon as that point is reached, they will get to the descending part of the graph, growing until they become visible. The ascending region between C and E does not difficult drop growth because for strongly supersaturated environments S always lies above the $S_r(r)$ curve there.

This shows that the mechanism of spontaneous drop formation also applies to electrically neutral condensation nuclei. Anyhow, charged drops require less supersaturation to be formed; charged particles are better condensation nuclei.

2.1.4 Dynamical analysis

The previous sections presented a static analysis that *ignored statistical fluctuations*. Taking into account, however, that a cloud chamber works under supersaturation conditions, fluctuations are expected to play an important role.

Specifically, looking at Figures 2.2 and 2.3, it is in principle possible that droplets of the ascending region, which are always present, will randomly fluctuate in size. If the supersaturation is high, and the droplet has a relatively large radius, such fluctuations could be large enough to bring it to the descending region, where it would grow until reaching a visible size.

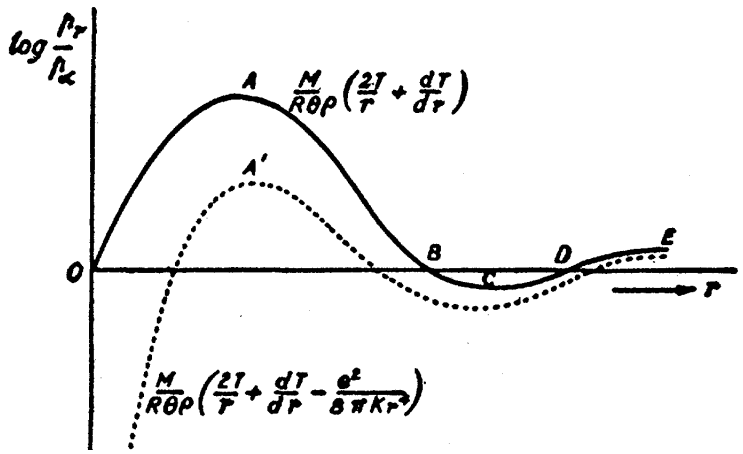

Figure 2.3: Vapour pressure for drops adding a dependence of surface tension with radius. Here, T is the surface tension and θ the temperature. Unrationalized Gaussian electromagnetic units are used. The dotted curve shows how it looks for charged drops. Source: Ref. [22].

A quantitative study of statistical fluctuations for charged droplets with constant surface tension was carried out by A. Langsdorf as part of his Ph.D. thesis [25]. This analysis defined a half-life λ as the time interval in which half of the spontaneously formed charged droplets transverse the "barrier" from Figure 2.2; thus growing and reaching a visible size. λ was then estimated with the help of various variables and functions:

- A parameter $q \in [0, 1]$ defined as the ratio between the two critical radii r_c for a given supersaturation S. It is, thus, given by the ratio of the two real roots of equation (2.3).
- A function $Q(3)$ given by

$$Q(3) = (1-q)^3 \frac{1+4q+q^2}{q^2 \alpha_m}\,, \tag{2.5}$$

  α_m being an abbreviation for

$$\alpha_m = \sqrt{[}3]{\frac{q^3+q^2+q+1}{4}}\,. \tag{2.6}$$

- Another function $Q(7)$, given by a complicated numerical expression. In the reference, a few values of $Q(7)$ are calculated for different $q \in [0, 1]$. These values have been fitted to a logarithmic law, obtaining

$$Q(7) = (-3.611 \pm 0.007) + (-2.00 \pm 0.02) \log_{10} q\,, \tag{2.7}$$

  with a high correlation coefficient equal to 0.9996 that indicates the suitability of the fit.
- The number μ of molecules in a drop whose radius is given by the maximum of Figure 2.2:

$$\mu = \frac{e^2 \rho N_A}{12\pi\varepsilon\gamma M}\,, \tag{2.8}$$

  where N_A is Avogadro's number.

- The critical supersaturation S_c given by equation (2.4).

With these definitions, the half-life λ is given by:

$$\log_{10}\lambda = -\log_{10} S - \log_{10}\left[\varepsilon^{1/9}\left(\gamma|_{\mathrm{dynes/cm}}\right)^{4/9}\left(M|_{\mathrm{g}}\right)^{1/2}\left(p_\infty|_{\mathrm{dynes/cm^2}}\right)\left(\rho|_{\mathrm{g/cm^3}}\right)^{-1}\left(T|_{\mathrm{K}}\right)^{-5/6}\right] + Q(7) + Q(3)\frac{1}{6}(\log_{10} e)(\mu \ln S_c) \pm 0.1\,. \tag{2.9}$$

The main subtlety is that the quantities in square brackets must go in CGS units. As is shown in the reference, the formula has an estimated error of around 0.1. This equation has been used to numerically calculate the half-life for isopropanol at different temperatures, obtaining the results of Figure 2.4.

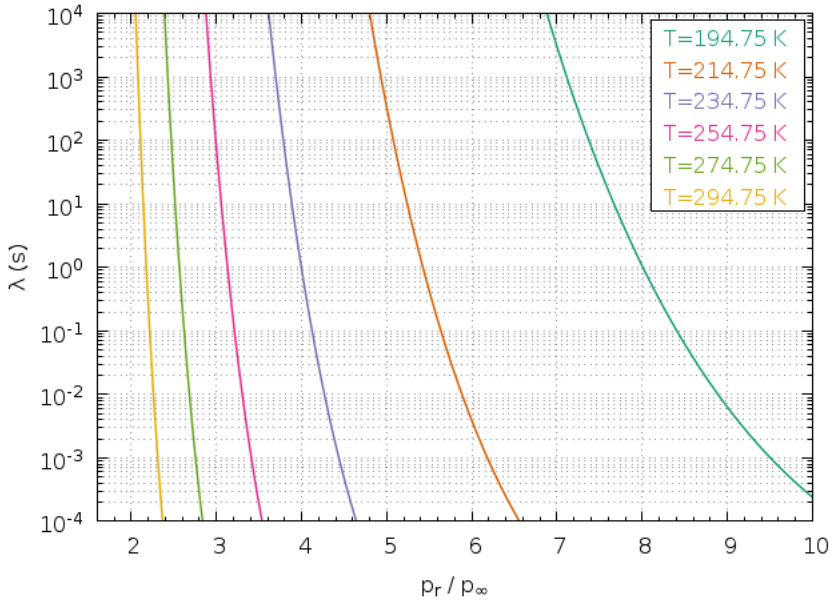

Figure 2.4: Condensation life-time for isopropanol. Notice the vertical logarithmic scale.

As might have been expected, λ has a strong dependence on the temperature. The most significant aspect of the plot, however, is the extremely high variation of the life-time with supersaturation. In other words, there is a maximum supersaturation, which goes from about 8 at 194.75 K to about 2.1 at 294.75 K, at which this phenomenon exponentially stops playing an important role.

2.1.5 Drop growth

Once the supersaturation is high enough for drop growth to be spontaneous, it is easy to estimate the rate at which drops will grow. According to J.G. Wilson [26], if r_0 is the radius of the drop, its rate of change with time is given by

$$\frac{dr_0^2}{dt} = \frac{2D}{\rho}(\rho - \rho_0) \simeq 2D\,, \tag{2.10}$$

where D is the diffusion coefficient of the vapour on the surrounding gas and ρ_0 the density of the vapour far from the drop. The constancy of the expression (2.10) was experimentally verified by W.E. Hazen [27].

From a quantitative point of view, equation (2.10) gives a growth rate for r_0^2 of around $8 \cdot 10^{-6}$ m^2/s for temperatures between $200 - 300$ K. Since, according to Figure 2.2, drops are formed with a radius $r \sim 10^{-9}$m and, as reported by Ref. [22], the limit of unaided vision is $5 \cdot 10^{-5}$ m, it takes about $3 \cdot 10^{-4}$ s for a drop to reach a visible size.

Even though this time may seem negligible, it is not if it is considered that ionising radiation is, as will be seen in the next subsection, usually moving at relativistic speeds. Consequently, in the time required for drop growth, particles will have travelled a distance of about 10 km; *tracks formed inside a cloud chamber are not live pictures of passing particles.*

2.2 Ionisation and track formation

The analysis of drop formation is essential to understand the physics behind cloud chambers. Nevertheless, it must never be forgotten that drops that in these devices form tracks grow on ions created by the passage of ionising particles. Thus, this ionisation process must be analysed.

According to experimental data [28, 29] the specific ionisation dN/dx in cloud chambers, defined as the mean number of ions produced per unit of length by a passing particle, is well described to a first approximation both for electrons and for more massive particles by the Bethe equation for restricted energy transfers [30]

$$\frac{dN}{dx} = \frac{\rho}{W} K z^2 \frac{Z}{A} \frac{1}{\beta^2} \left[\frac{1}{2} \ln \left(\frac{2 m_e c^2 \beta^2 \gamma^2 W}{I^2} \right) - \frac{\beta^2}{2} \left(1 + \frac{W}{T_{\max}} \right) - \frac{\delta}{2} \right] , \tag{2.11}$$

where

- ρ is the density of the ionised gas.
- W is the average energy required to produce an electron-ion pair, tabulated in [31]. It does only slightly depend on the energy and nature of the particle, being the dependence on them logarithmic. It is about 37 eV for air and about 25 eV for small organic molecules such as isopropanol. Because of the form of the dependence of equation (2.11) on W, the precise value of the latter does not affect the order of magnitude of the result.
- $K = 4\pi N_A r_e^2 m_e c^2 = 0.307075$ MeV g^{-1} cm^2. r_e is the classical electron radius.
- z is the charge, in units of the electron charge, of the incident particle.
- $\frac{Z}{A}$ is the ratio between the atomic number and atomic mass of the absorber.
- $\beta = v/c$ is the speed of the incident particle divided by the speed of light.
- m_e is the electron mass.
- γ is the Lorentz factor.
- I is the mean excitation energy of the absorber, tabulated in [32]. Its value for air is 85.7 eV and for isopropanol 61.1 eV.
- $T_{\max}$ is the maximal possible energy transfer, of order $m_e c^2 \gg W$.

- δ is the density effect factor, a correcting term that takes into account the polarization of the medium as the particle travels through it. Only significant at high energies, it is usually parametrised with values tabulated in Ref. [32]. For the specific parametrisation, see Ref. [30].

This equation accounts for the energy transfers below W. It may be expected to work better than the usual Bethe equation because the latter includes very rare events with large single-collision deposits [30].

As can be seen, there is no dependence on the mass of the incident particle, just on its charge. The results for $z = \pm 1$ (e.g., $e^{\pm}$ and $\mu^{\pm}$) and $z = 2$ (e.g., α particles) both for isopropanol and air at $T = 200$K and $P = 1$ atm can be seen in Figure 2.5.

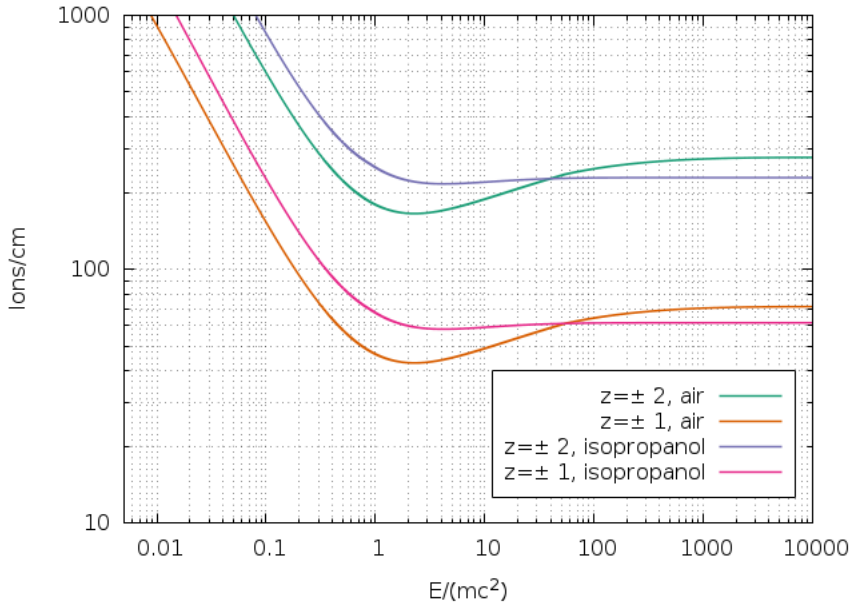

Figure 2.5: Specific ionisation for different charges and absorbing media. The intersection between the air and isopropanol curves is due to the density effect factor.

There are some remarkable aspects of this result. First of all, *cloud chambers will mostly detect relativistic particles*, for which $E \sim mc^2$: the mass of the incident particle fixes a natural energy scale. For non-relativistic particles, the energy lost per cm by ionisation will be exponentially large, and the particles will be easily stopped. For a given energy, therefore, more massive particles have lower ranges. This is the case of, for instance, α particles, whose range in air at standard conditions is about 2 cm to 10 cm. Furthermore, for any particle the ionisation increases with z through a factor z^2.

Qualitatively the result is, on the other hand, almost independent of the absorbing medium. The most remarkable aspect is a dependence on ρ which, in the case of gases, means that high pressures and low temperatures favour ionisation.

To sum up, the preceding results show that if the supersaturation inside the chamber is high enough, *every single charged particle will act as a condensation nucleus*. What is more, the amount of ions that any passing particle creates is, under normal working conditions, about 100 per centimetre. That is, for a high enough supersaturation every passing charged particle *will leave a macroscopically visible track*.

2.3 Operating conditions inside a diffusion cloud chamber

Turning back to condensation, all the presented models suggest that high temperatures favour it, requiring less supersaturation for drop formation. In cloud chambers, however, a low temperature is responsible for taking the vapour into its supersaturated state. What is more, the vapour pressure p_∞ exponentially decreases with decreasing temperature [16]; thus a good temperature gradient is in principle enough to effectively attain a high supersaturation at the bottom of the chamber.

Anyhow, the importance of different factors show that to adequately analyse the optimum working conditions a collective model that predicts the supersaturation distribution inside the chamber is unavoidable. Such an analysis was both carried out and experimentally verified by P.E. Argan et al. in Ref. [33]. A study of the conditions inside a cloud chamber based on their theoretical formulae will be presented in this section.

Their model makes several assumptions, the most important being the consideration of stationary operation, which neglects the dynamical convection phenomena that may happen inside the chamber but gives anyway a general idea. Vapour removal by drop formation is as well neglected as a first approximation. Their original analysis is also one-dimensional, neglecting side-wall effects. Although a bi-dimensional model is also worked out, the typical dimensions of the home-made cloud chambers that are analysed in this thesis make a one-dimensional model appropriate enough.

2.3.1 Temperature distribution

If the bottom and top temperatures, T_0 and T_1, are fixed, the temperature distribution in the cloud chamber is predicted to be given by

$$T(y) = T_0 + \frac{1 - e^{-ay}}{1 - e^{-ah}}(T_1 - T_0)\,, \tag{2.12}$$

where:

- $T(y)$ is the temperature at height y, $y = 0$ corresponding to the bottom of the chamber.
- h is the height of the chamber.
- $a = \frac{C_P P D_1}{\kappa R T_0^2}\Gamma$, with:
  - C_P the specific heat of the vapour at constant pressure.
  - P the working pressure inside the cloud chamber, which in most or all cases will be 1 atm.
  - D_1 the diffusion coefficient of the vapour inside the gas at temperature T_1.
  - κ the heat conductivity of the vapour-gas mixture. It can be estimated using, for instance, the formula given by Mason and Saxena in Ref. [34].
  - Γ a parameter whose definition will be clear in the next subsection, given by

$$\Gamma = \frac{T_1 - T_0}{h}\frac{\ln\left[1 - \frac{p_\infty(T_1)}{P}\right]}{\ln(T_0/T_1)}\,; \tag{2.13}$$

    $p_\infty(T)$ stands for the vapour pressure of the diffusing vapour at temperature T.

The results can be seen in Figure 2.6.

It is notable that most distributions do not extremely differ from the linear temperature distribution that corresponds to the $ay \ll 1$ limit. However, with the distribution being concave, the

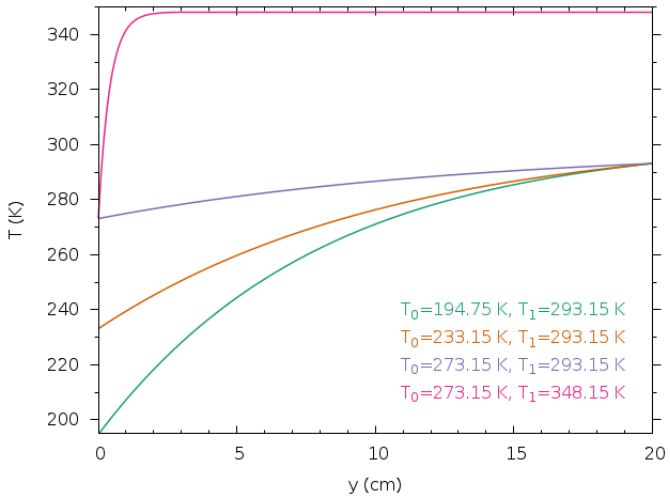

Figure 2.6: Temperature distribution inside a diffusion cloud chamber for different bottom and top temperatures. Data for isopropanol and $h = 20$ cm has been used.

temperature inside the chamber will always be higher than if its behaviour were linear. Since $1/p_\infty$ is a decreasing function of temperature [16] and therefore—in principle—S as well, low temperatures are desirable: *optimum working conditions will generally look for a linear behaviour and make the parameter a small.*

Interestingly, the results show a strong departure from linearity when the upper temperature T_1 is high. This phenomenon is explained by the strong dependence of a on T_1 through the factor

$$\ln\left[1 - \frac{p_\infty(T_1)}{P}\right], \tag{2.14}$$

which is plotted for isopropanol in Figure 2.7.

This function has the undesirable property that as the temperature gets closer to the boiling temperature (355 K for isopropanol), a diverges. Therefore, a naive increase of the temperature gradient by heating the upper surface does not lead to a higher supersaturation if T_1 approaches the boiling temperature of the vapour. Intuitively, this behaviour can be explained noting that at the boiling point, $p_\infty = P$; thus close to it, the molar fraction of the vapour rises exponentially. Consequently, a high amount of hot vapour enters the chamber, heating it.

In short, not only a temperature gradient is important, but also a top temperature far from the boiling point. *Cooling the bottom surface is more important than heating the top.*

2.3.2 Supersaturation distribution: a first approximation

Even though the study of the temperature distribution inside a cloud chamber is interesting as a first analysis, the single most important parameter is the supersaturation distribution $S(y)$. With it, the height of the layer in which spontaneous condensation on charged nuclei and track formation take place can be estimated.

Under the same hypotheses that led to the temperature distribution, Argan et al. showed that the supersaturation distribution inside a diffusion cloud chamber is given by

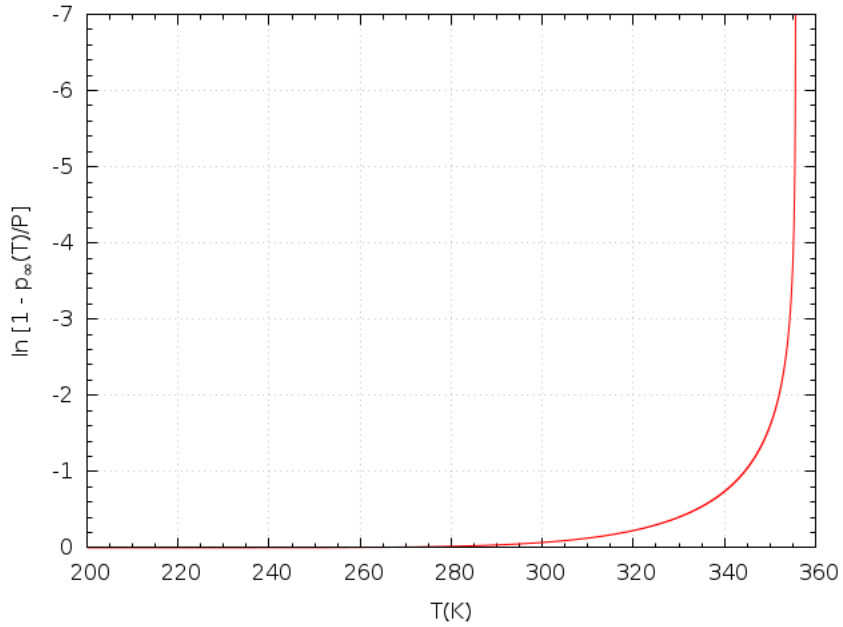

Figure 2.7: Behaviour of the $\ln\left[1-\frac{p_\infty(T_1)}{P}\right]$ factor for isopropanol and $P = 1$ atm. Its negative sign compensates with the negative value of $\ln(T_0/T_1)$.

$$S(y) = P\frac{1 - T_0^{\Gamma/A}[Ay + T_0]^{-\Gamma/A}}{p_\infty(T(y))}\,, \tag{2.15}$$

where $A = (T_1 - T_0)/h$. Γ is the same parameter that was previously defined, which is in fact obtained by requiring the top part to be strictly saturated with vapour, that is, $S(h) = 1$.

This distribution for different bottom and top temperatures is given by the continuous curves in Figure 2.8. The dotted curve represents the critical supersaturation S_c for which every single charged particle acts as a condensation nucleus that grows until it reaches a visible size. The dot-dashed curve represents the supersaturation for which the "half-life" after which a spontaneously formed microscopic droplet reaches a visible size is 1 s. Consequently, the region between the intersections of the continuous curve with the dotted curves represents the region in which tracks will be formed; *the sensitive layer of the cloud chamber*.

As can be seen, for bottom temperatures $T_0 \lesssim 230$ K, this layer has an appreciable height. In addition, the region in which drops are formed by statistical fluctuations and not by spontaneous condensation becomes important for $T_0 \sim 230$ K, being irrelevant for lower bottom temperatures. For higher bottom temperatures such as $T_0 = 273.15$ K, however, not even $S = 1$ is attained; there is no track formation inside the chamber. Increasing the top temperature in that case slightly increases S, though the effect is completely negligible. 293.15 K seems in all the analysed cases an adequate upper temperature.

2.3.3 Supersaturation distribution: considering vapour removal

There is a striking phenomenon that is observed in Figure 2.8 that has not been mentioned: a ridiculously high supersaturation is predicted for bottom temperatures $T_0 \lesssim 210$ K. This aspect

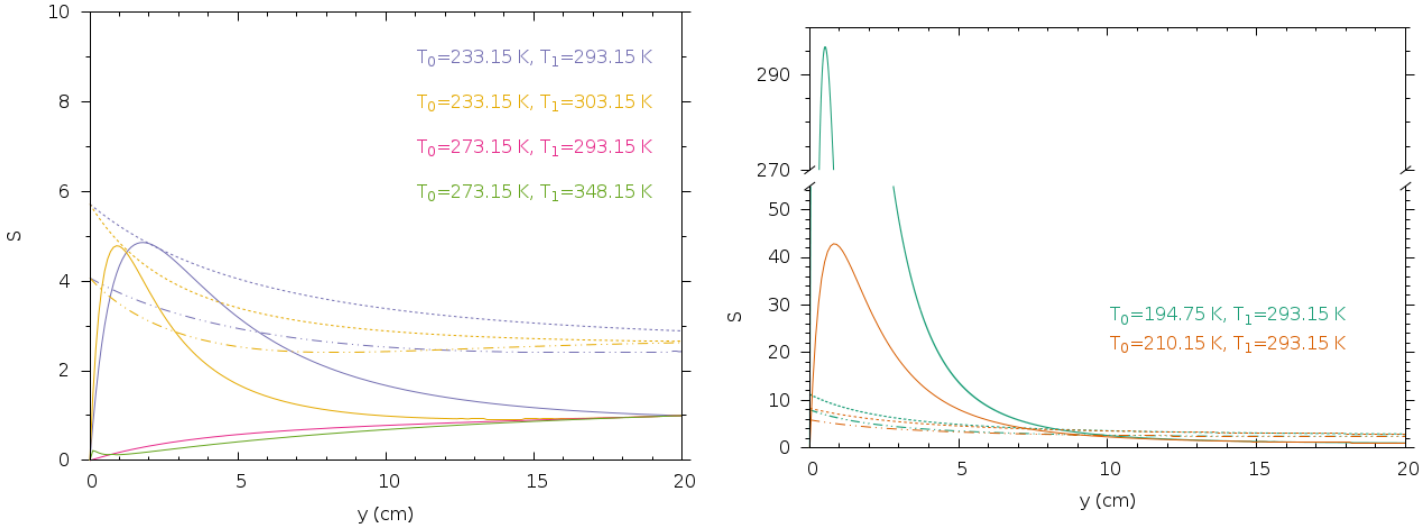

Figure 2.8: Supersaturation distribution for different bottom and top temperatures. Data for isopropanol has been used.

raises a question about the validity of neglecting vapour removal by drop formation for constructing the model. Because of that, Argan et al. developed an iterative method that takes it into account.

The procedure starts by assuming a value ϵ for a parameter that represents the fractional decrease in the vapour flux at the bottom of the chamber due to condensation. Denoting by ξ the depth of the sensitive layer, the algorithm is as follows:

1. A parameter ϵ' is defined as:
$$\epsilon' = \frac{1-\epsilon}{\xi}\,. \tag{2.16}$$

2. A parameter η' is defined as:
$$\eta' = \frac{\epsilon'(A\xi/T_0 - 1)}{\epsilon'\xi - 1}\,. \tag{2.17}$$

3. The new temperature and supersaturation distributions are assumed to be given by
$$T(y) = (1+\eta' y)T_0(y)\,, \tag{2.18}$$
where $T_0(y)$ is the temperature distribution given by equation (2.12), and
$$\ln\frac{P - S(y)p_\infty(T(y))}{P - p_\infty(T_0)} = -\frac{\Gamma}{T_0}y\left[(1-\epsilon'\xi) + y\left(\epsilon' - \frac{1}{2}\frac{A}{T_0}\right)\right]\,. \tag{2.19}$$
The last two equations are valid for $y < \xi$, that is, for the region in which there is vapour removal because of drop formation.

4. After a new supersaturation distribution has been obtained, a new value for ξ can be calculated. Updating the value of ϵ as
$$\frac{1-\epsilon_{\text{old}}}{1-\epsilon_{\text{new}}} = \frac{\xi_{\text{old}}}{\xi_{\text{new}}}\,, \tag{2.20}$$
the process may be repeated until it converges.

The results for different bottom and top temperatures and different initial values for ϵ are plotted in Figure 2.9. Again, these results show the importance of obtaining a low bottom temperature. *Even small reductions of the gradient by lowering the top temperature do not lead*, as can be seen, *to significant differences*. It is as well remarkable that for very low bottom temperatures large supersaturations are still predicted even when taking into account vapour removal. This supersaturation may lead to a formation of mist that could reduce the visibility inside the chamber.

What is more, it is also seen that excessive vapour removal leads to a destruction of the sensitive layer. Therefore, it is essential to *avoid any preventable vapour removal*, either due to condensation on irregular objects placed inside the chamber or due to leaks that result from an imperfect sealing.

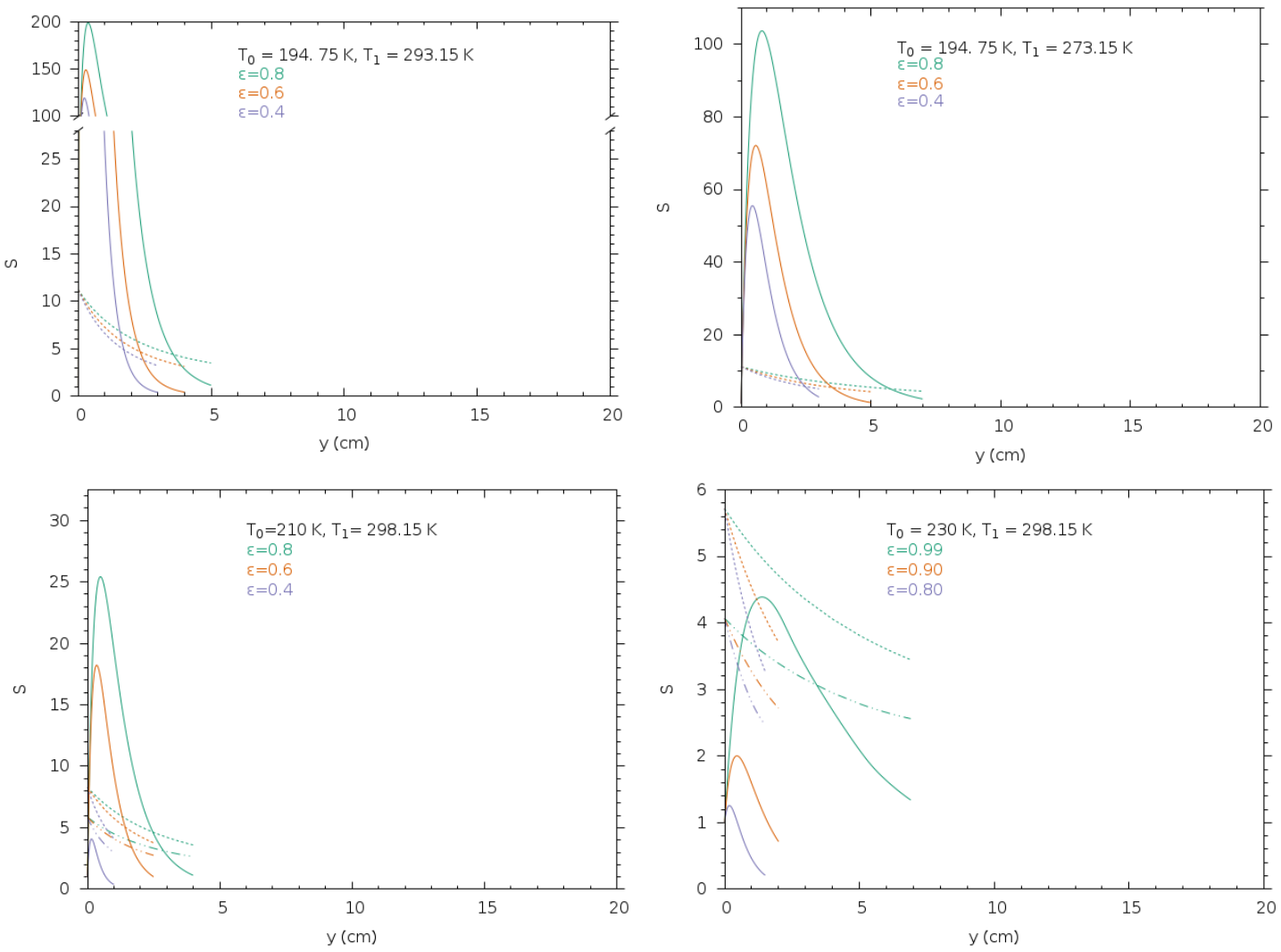

Figure 2.9: Supersaturation distribution in the sensitive region for different temperature configurations. According to Argan et al., ϵ usually lies between 0.6 and 0.8. Distributions in which there is no sensitive region indicate that the iterative process ended within that situation.

Estimation of the parameter ϵ

Even though the presented algorithm seems to give a definite answer to the problem of estimating the working conditions inside a diffusion cloud chamber, there still remains a free parameter, ϵ, that should be at least estimated. Argan et al. give a numerical approximation for it. Nevertheless, being just a rough estimation it is more important to note the following properties they derived:

- ϵ is usually between 0.6 and 0.8.
- $1 - \epsilon \propto \frac{\rho R T_1^2}{M D \Gamma}$, what means that small molecular masses, small values of Γ, and high upper temperatures favour vapour removal and are thus undesirable.

2.4 Comparison of different vapours

After the physical conditions inside a diffusion cloud chamber have been established, they can be used to compare different working conditions and choose the optimum ones. A significant choice that has to be made when designing a diffusion cloud chamber is the vapour that will be used for condensation. In this section, three common organic alcohols will be compared: isopropanol, methanol and ethanol.

There are two important expressions in which the nature of the specific vapour plays a fundamental role:

1. In the determination of the temperature distribution, the combination $\frac{C_P D}{\kappa}$ appears, being preferably small to obtain a better temperature gradient.
2. In specifying the critical supersaturation needed for spontaneous drop formation, the expression $\frac{M\gamma}{\rho}$ appears. A small value is equivalent to raising the temperature, which reduces the critical supersaturation and is thus desirable.

The values of both quantities for isopropanol, methanol and ethanol are given in Table 2.1.

	$C_P D/\kappa$	$M\gamma/\rho$
Isopropanol	0.73	$2.24 \cdot 10^{-6}$
Ethanol	0.88	$1.78 \cdot 10^{-6}$
Methanol	1.01	$1.22 \cdot 10^{-6}$

Table 2.1: Comparison of different vapours

The combination

$$\ln\left[1 - \frac{p_\infty(T_1)}{P}\right] \tag{2.21}$$

also appears when determining both the temperature and supersaturation distributions. However, as can be seen in Figure 2.10, it does not significantly differ at common working temperatures between different organic vapours. It is noticeable, though, that at room temperature the factor is about two times larger for methanol than for isopropanol or ethanol.

A remarkable conclusion is that isopropanol is the vapour that leads to better temperature distributions, a property that is enhanced by the small values that $\ln\left[1 - \frac{p_\infty(T_1)}{P}\right]$ takes. What is more, its evaporation rate is approximately twice as high as the one of ethanol, thus reaching the equilibrium distribution faster [16]. This last property is probably due to its higher molecular

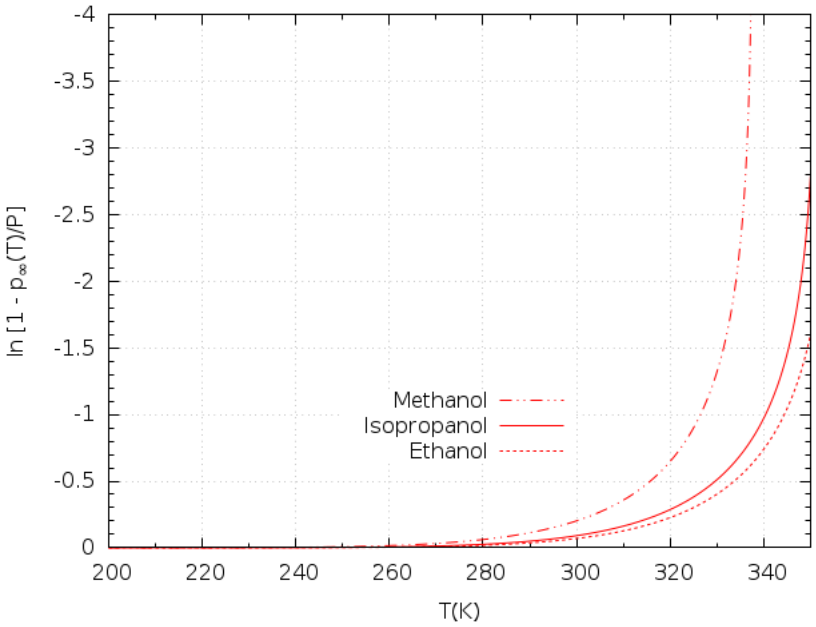

Figure 2.10: Variation of Γ for different vapours. $P = 1$ atm.

mass, since according to the Hertz-Knudsen-Langmuir equation the evaporation rate is higher for gases with more massive molecules [35].

Nevertheless, if the temperature gradient is not strong enough, and thus the supersaturation inside the chamber is small, a lower critical supersaturation may be desirable. Therefore, ethanol or methanol may be preferable. In fact, professional references in which other factors such as temperature, pressure or stability are much better under control recommend using methanol [36], the alcohol with the smallest molecular mass. If the intended use is a pedagogical one, however, ethanol might be preferable to methanol, both because of being easier to obtain and because of the toxicity of the latter alcohol.

Chapter 3

Physics Insight. Observation and analysis

Having the physics of condensation inside a cloud chamber been studied, it is essential to analyse the main purpose for which diffusion cloud chambers were originally designed: the study of the properties of ionising radiation. As will be seen, however, it is difficult to carry out quantitative measurements in a diffusion cloud chamber without using sophisticated magnetic devices. The sections of this chapter that deal with deflection of particles by a magnetic field are thus included just for completeness.

3.1 Illumination

As has been established in the previous chapter, if the supersaturation inside the chamber is high enough, every passing particle will leave a macroscopically visible track. In order to effectively see it, a strong light source is needed, light that will be scattered by the drops. If there is enough contrast, that is, if the bottom of the chamber is dark enough, tracks will in principle be visible.

Nevertheless, when a light ray crosses a spherical drop, the various transmission and diffusion processes distribute the energy of the ray in all directions. Consequently, observation should not rely on diffused light; *an observation through reflection is desirable.*

To do so at large incident angles, which maximize reflectance, a scheme similar to the one in Figure 3.1 is advantageous. That configuration has the advantage as well that, in principle, any observation angle is reached by reflected light, though with a lower intensity for bigger angles.

3.2 Momentum measurement

The most immediate measurement that can be made with any particle tracker is the determination of the linear momentum using an homogeneous magnetic field. If a particle of charge ze describes a circle of radius ρ perpendicular to a magnetic field B, then its momentum p is given by

$$p|_{\mathrm{GeV}} \simeq 0.3\, z\, B|_{\mathrm{T}}\, \rho|_{\mathrm{m}}\ , \tag{3.1}$$

where the 0.3 proportionality constant is just 10^{-9} times the speed of light.

The measurement of ρ, taking into account the inclination of the image-taking device with respect to a plane perpendicular to the magnetic field, leads to a determination of the momentum p provided the magnetic field B is known.

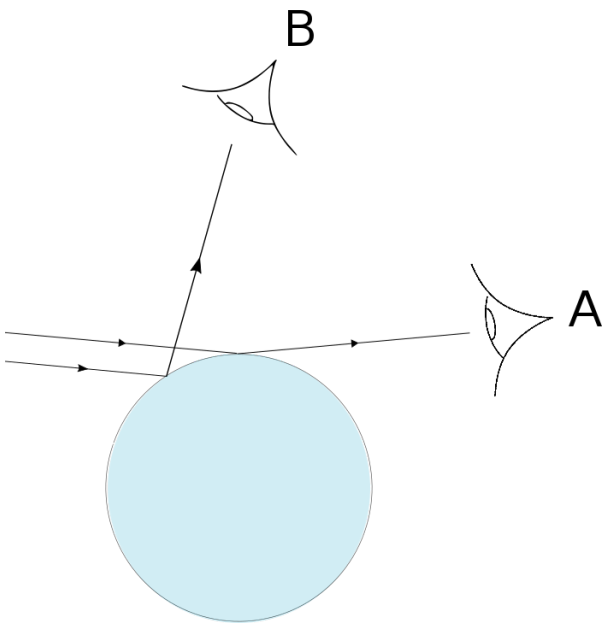

Figure 3.1: Ideal scheme for illumination, with grazing light. Observer A will see tracks more clearly, though observer B will also see them.

3.2.1 Large radii: the sagitta method

Equation (3.1), though clear and simple, has the problem that the curvature radius is usually much larger than the dimensions of the chamber. For instance, cosmic rays, whose energy[1] is of order GeV [11], have curvature radii of a few meters even for remarkably strong magnetic fields of order T. Because of that, and due to the experimental difficulty of having a strong uniform magnetic field over a wide area, even under the most favourable experimental conditions only an arc, and not a circle, will be observed.

In order to get the radius from a measurement of just a deflected track, the sagitta method [37] may be used. If L is the length of the chord determined by the extreme points of the arc described by the particle and s is the sagitta, the maximum distance between the arc and the chord (see Figure 3.2), then s is related to the radius of curvature ρ by

$$s = \rho \left[1 - \sqrt{1 - \left(\frac{L}{2\rho} \right)^2} \right] \approx \frac{L^2}{8\rho} + \mathcal{O}\left(\frac{L^4}{\rho^3} \right) , \tag{3.2}$$

and thus a determination of s, in principle measurable for any appreciable deflection, allows to obtain the curvature radius ρ.

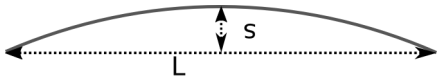

Figure 3.2: The sagitta method

[1] And, being relativistic, their momentum as well.

3.2.2 Momentum change: charge and energy loss

If the experimental conditions are good enough to allow a measurement of the momentum, the insertion of a dense metal plate, such as Pb, inside the chamber allows to quantify the momentum loss inside the plate by comparing the curvature between both sides [22][2]. Furthermore, this comparison determines the incident direction of the particle as the direction in which it loses momentum. The energy loss can as well be extracted if the mass of the particle is known. It is then possible to compare this loss to the Bethe equation (2.11) and thus verify its properties.

The direction of curvature together with the incident direction also allows to obtain the sign of the electric charge of the particle. This measurement led, for instance, to the discovery of the positron [3].

This technique, though, has the disadvantage that introducing a plate inside a diffusion cloud chamber increases the vapour removal by condensation, which, as has been shown in Section 2.3.3, leads to a worsening of the supersaturated sensitive region.

3.2.3 Errors and possible field sources

Although the results presented in this section could lead to the conclusion that momentum determination is an easy and powerful technique, the nature of diffusion cloud chambers makes it hard to be employed. The main problem is that gas motion leads, even for expansion cloud chambers, to distortions in particle tracks that might be confused with magnetic field curvatures. These distortions are magnified in diffusion cloud chambers due to the high temperature gradient.

Because of that, any rigorous analysis must include a calibration of the displacement of tracks inherent to the chamber, without any external magnetic field. This displacement is about 2 mm in expansion cloud chambers, introducing an error of 6% when $p = 1$ GeV and of 100% for $p = 20$ GeV, but can be considerably higher for diffusion cloud chambers.

What is more, the calibration must be carried out under the same experimental conditions that will be used with an external magnetic field. In principle, electromagnets, whose field can be turned off, seem therefore the most appropriate devices for cloud chambers.

Furthermore, the required strength and homogeneity properties in order to get appreciable sagittas demand powerful coils, which must be as isolated as possible from the chamber to avoid causing convective currents[3]. Consequently, *small chambers are virtually the only ones suitable for momentum determination.*

3.3 Mass determination

Once the momentum has been measured, there are at least three techniques that allow to determine the mass of the passing particle. The techniques, more or less appropriate depending on the nature of the analysed particle, are discussed below.

3.3.1 Momentum and range

Particles that are stopped by energy losses due to ionisation provide, through their range, a way of measuring their mass.

The method is based on the fact that momentum and range share the common property that they only depend on $\beta\gamma$, where $\beta = v/c$ and γ is the Lorentz factor. Moreover, their dependence

[2] Most of the information in this section, as well as in Sections 3.2.3 and 3.3, has been extracted from Ref. [22].

[3] When expansion cloud chambers were used for the study of cosmic rays, the cooling of powerful electromagnets that reached even 1.5 T was the most important technological challenge.

on the mass of the ionising particle is in both cases linear. Because of that, the quotient $B\rho/R$, where ρ is the radius described under a magnetic field B and R is the range of the particle, is only a function of $\beta\gamma$, not of the mass of the particle:

$$\frac{B\rho}{R} = zeb\frac{\beta\gamma}{\frac{2+\beta^2\gamma^2}{\sqrt{1+\beta^2\gamma^2}} - 2}\,. \tag{3.3}$$

ze is the charge of the particle and b a constant given by

$$b = \frac{e}{c}\rho K\frac{Z}{A}\frac{1}{2}\ln\left(\frac{2m_e c^2 W}{I^2}\right)\,, \tag{3.4}$$

the symbols having been defined in the restricted Bethe equation (2.11).

Inverting equation (3.3) allows an experimental determination of $\beta\gamma$ and, since

$$p = Mc\beta\gamma\,, \tag{3.5}$$

and

$$R = \frac{Mc^2}{Z^2 a}\left(\frac{2+\beta^2\gamma^2}{\sqrt{1+\beta^2\gamma^2}} - 2\right)\,, \tag{3.6}$$

being M the mass of the incident particle, the knowledge of either the momentum or the range allows, by determining $\beta\gamma$, to measure the mass of the ionising particle.

It is important to mention that for deriving the expression (3.6) the logarithmic variation with $\beta\gamma$ and the β^2 term in the square brackets of equation (2.11) have been neglected. A more accurate calculation could therefore numerically integrate equation (2.11) to obtain a more precise dependence on β of the range R:

$$R = \int\frac{dE}{-dE/dx} = \int\frac{\beta c\,dp}{W dN/dx} = Mc^2\int\frac{\beta\gamma^2\,d\beta}{W dN/dx}\,. \tag{3.7}$$

3.3.2 Rate of change of curvature

As has been described in Section 3.2.2, the insertion of a metal plate and the measurement of the momentum on each side can contribute to the study of the properties of the incident radiation. In particular, it helps to determine the mass of particles that are not stopped by energy losses due to ionisation.

From a more quantitative point of view, it can be shown that the rate of change of $B\rho$, related through equation (3.1) to the rate of change of momentum, is given by

$$\frac{d(B\rho)}{dx} = \frac{1}{zec}\frac{1}{\beta}\frac{dE}{dx}\,, \tag{3.8}$$

a function of the speed of the incident particle, not of its mass. Thus, by measuring the difference in $B\rho$ between both sides of the plate, the initial speed of the particle can be obtained and, with equation (3.5), its mass.

3.3.3 Method of elastic collision

The presented methods have the problem that they rely on the Bethe equation, an expression that gives the average energy loss and may need corrections if an improved accuracy is desired.

There is, however, a technique that only relies on the principles of energy and linear momentum conservation. It requires, nevertheless, the observation of an elastic collision between the incident particle and an electron. It can be shown that if T is the kinetic energy imparted to a free electron, emitted at an angle θ with respect to the incident particle, then

$$T = 2m_e c^2 \frac{p^2 c^2 \cos^2\theta}{\left[m_e c^2 + \sqrt{p^2 c^2 + M^2 c^4}\right]^2 - p^2 c^2 \cos^2\theta}\,, \tag{3.9}$$

being p the momentum of the incident particle before the collision and M its mass. The measurements of the momenta before and after the collision, thus, allow a direct determination of M.

This method, however, has the disadvantage that the collision must have a high energy-transfer in order to see the track of the emitted electron. For energetic particles, this is a rare phenomenon.

3.4 Qualitative reactions

Apart from the quantitative measurements described, there are some processes that can be qualitatively observed in any cloud chamber:

- *Stopping of α particles*: α particles, having a high mass and a charge $z = 2$, lose a lot of energy because of ionisation and are stopped even by few centimetres of air. Because of that, in a cloud chamber they can be identified as thick tracks that stop after a few centimetres.
- *Collisions*: two tracks that converge to one can be identified as a signal that an incident particle has hit an electron inside the chamber.
- *Multiple scattering*: a track that "zig-zags" is characteristic of a low-energy particle that is multiple-scattered by the nuclei of the gas inside the chamber.

There are some references that assert that it is possible as well to observe a muon decay:

$$\mu^- \to e^- + \nu_\mu + \bar{\nu}_e\,. \tag{3.10}$$

A sharp, straight track that abruptly changes its direction would be a signal of this process. Nevertheless, the probability P of observing such a decay in a track of length L is given by

$$P = 1 - e^{-\frac{L}{c\tau}} = 1 - e^{-1.52\cdot 10^{-5}\frac{L|_{\text{cm}}}{\gamma}} \simeq 1.52\cdot 10^{-5}\frac{L|_{\text{cm}}}{\gamma} + \mathcal{O}\left(\left(\frac{L|_{\text{cm}}}{\gamma}\right)^2 \cdot 10^{-10}\right)\,, \tag{3.11}$$

τ being the lifetime of the muon in the laboratory frame and γ being the Lorentz factor. The muons are supposed to move at a speed c because for cosmic rays their energy is of order GeV [11], e.g., more than 10 times their mass. This probability P is always smaller than 10^{-4} for $L \sim 10$ cm. Taking into account that the number of events per second is expected to be of order ~ 1 or less, the probability of observing this decay is negligibly small. Thus, apparent deflections may be more likely attributed to vapour currents or scattering processes.

Chapter 4

Experimental insight. Results of an empirical study

In order to complement the theoretical results from the previous chapters and to provide experimental data and graphical results, a diffusion cloud chamber was built in the Theoretical Physics and History of Science Department.

Even though the basic conditions were always the same, isopropanol diffusing in air with a bottom surface cooled with dry ice, different configurations were tested. With that, the advantages and disadvantages of various experimental conditions were established.

Finally, in this thesis diffusion cloud chambers are studied from a particle physics perspective, where they are very interesting pedagogically. Because of that, both images and videos of phenomena regarding cosmic rays and particles from radioactive sources were recorded and are presented.

4.1 General building guidelines

4.1.1 Materials

The procedure that proved to be more effective and efficient requires the following material:

- A transparent, rigid container with flat sides and an open bottom to form the structure of the chamber. In this project, its dimensions were 20 cm $\times$ 20 cm $\times$ 30 cm.
- A metal plate, slightly bigger than the open face of the container (by about 5 cm is enough). The plate used in this thesis was made of stainless steel, its dimensions being 25 cm $\times$ 35 cm $\times$ 3 mm.

  Ideally it should be black to get a better contrast with tracks, though it can be covered either with black tape or with another thin black metal plate. In this project, a black coated aluminium plate was used for this purpose.

  The role of the large metal plate is to work as the cold surface of the chamber, while acting as well as a heat sink due to its bigger dimensions. That way, a strong temperature gradient can be maintained inside the chamber for a long enough time to reach a steady-state distribution.
- Pure isopropanol.
- Duct tape.

- A wide sponge, to be used as the isopropanol reservoir.
- A strong light source, ideally with a well-defined and orientable illumination direction. An overhead projector is a good option.
- Dry ice, as well as a suitable container for it to be used as the cold thermal reservoir. The cover of the original dry ice container is usually appropriate for this.

The materials used in this project can be seen in Figure 4.1.

Figure 4.1: Elements used for building the home-made cloud chamber. The dry ice is inside the box at the background of the left image. In subsequent tests, other sponges and plates were also used.

4.1.2 Procedure

With all the materials prepared, the procedure is as follows:

1. The chamber is thoroughly cleaned with isopropanol to remove any dirt or dust that may remove vapour and disturb the experiment.
2. The sponge, after being fixed with duct tape to the top of the chamber, is soaked with isopropanol.

   It is important to add the isopropanol in the center of the sponge, because otherwise it can remove the glue from the tape and thus make the sponge fall. It is also a common mistake to add too much isopropanol, between 30 ml and 40 ml being more than enough for the dimensions of the chamber used in this project.
3. The bottom, open face of the chamber is put on top of the metal plate, adjusting the joint with duct tape.
4. Everything is put on top of the dry ice container.

5. The illumination is adjusted so that, as explained in Section 3.1, light hits at grazing angles. To check this point, looking at small angles should allow to see a layer of mist at the bottom of the chamber if the illumination is correct.

   It is useful to surround the chamber with black cloth to minimize reflections from the outside.

6. After 15-20 minutes, tracks begin to appear.

7. Tracks continue to be seen for about an hour or even more. Their quality slowly decreases while the chamber cools down and the gradient disappears.

The experimental setup can be seen in Figure 4.2.

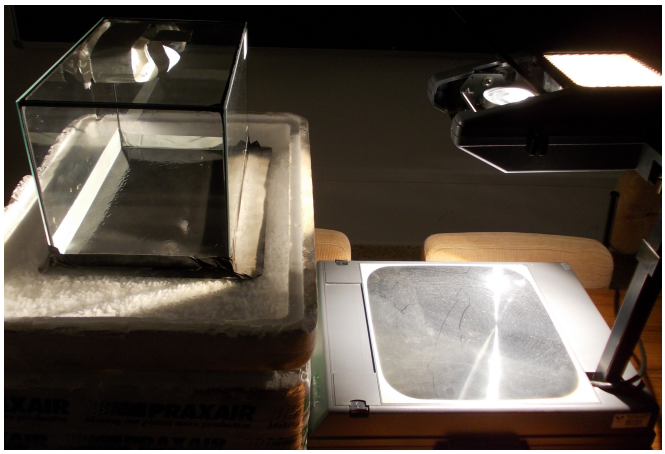

Figure 4.2: An effective setup for home-made cloud chambers. This specific test used paper instead of a sponge for the reservoir.

4.2 Temperature and different orientations of the chamber

4.2.1 Qualitative results

Even though the described procedure was found to be the optimum one, it would be interesting to use a configuration in which the open part of the chamber is placed on top. This last arrangement will be called "inverted configuration", whereas the usual one will be called "standard configuration".

The main benefit of the inverted configuration is that it enables an easy manipulation of the setup without having to disassemble it. This would allow, for instance, to refill the reservoir, increasing the durability of the chamber, or to add objects such as radioactive sources or magnetic devices. In few words, the experimental study would be significantly simplified.

That configuration has the problem, however, that it places a more or less thick glass layer between the dry ice and the inside of the chamber. Being glass a good thermal insulator, the necessary temperature gradient could then be difficult to attain.

This is, in fact, what was observed: in the inverted configuration, initially—after around 15 minutes— tracks began to be visible. However, the quality of the supersaturated layer soon decreased. This last result may be attributed to vapour removal: as has been shown in Section 2.3.3, it has the effect of reducing the supersaturation. For small gradients as the one created in the inverted configuration, this reduction leads to the disappearance of the sensitive layer.

What is more, as time advanced, the reservoir began to slowly cool. Although the theoretical results have shown that this should not significantly affect the steady-state distribution (see, for instance, Figure 2.9), it is in principle reasonable that this cooling may have a negative effect on the evaporation rate, reducing it and not reaching an equilibrium distribution.

The same effect was observed if a heat source, which was just a pot with water at 50°C, was placed on top in the inverted configuration (Figure 4.3). In this case, some tracks of alpha particles, the most ionising ones, could be seen as soon as 5 minutes after setting the experiment. However, the sensitive layer soon disappeared.

The early appearance of tracks may be attributed to the strong temperature gradient and the increase in the vapour pressure of isopropanol with respect to atmospheric pressure when this substance is close to its boiling point. Nevertheless, the supersaturation rapidly disappears due to the effect noted in Section 2.3.1, that when the upper temperature grows near to the boiling temperature of the diffusing vapour, the equilibrium distribution does not create a strong enough temperature gradient.

Figure 4.3: Configuration with a heat source on top. The white foam was holed to allow direct heat transfer between the source and the reservoir.

4.2.2 Quantitative results

In order to quantify the difference between the standard and inverted configurations, the temperature at different heights y of the chamber was measured for different times t with a thermocouple attached to a multimeter.

The results can be seen in Tables 4.1, 4.2 and 4.3. The temperatures were measured on the outside, so the results are only to be taken as estimations. The distribution was virtually homogeneous in the horizontal directions, being the differences of at most 1°C.

The data show that *the standard configuration undoubtedly is the one that better achieves a sustained temperature gradient.* In the inverted configuration, the gradient was not strong enough to create a permanent sensitive layer, whereas adding a heat source reduced the gradient after a while.

t \ y	5 cm	10 cm	15 cm	20 cm
5 min	20.5	21.6	22.0	22.3
10 min	17.5	18.9	20.6	23.0
15 min	7.5	13.5	16.0	20.0
20 min	5.0	15.0	16.5	18.0
25 min	8.0	15.0	17.2	19.0
30 min	9.5	15.2	17.2	19.0
45 min	9.3	14.5	16.5	19.0
60 min	6.0	15.0	19.0	19.9

Table 4.1: Evolution of the temperature distribution, in °C, for the standard configuration.

t \ y	0 cm	5 cm	10 cm	15 cm	20 cm
10 min	-9.0	17.0	20.0	21.0	22.0
15 min	-17.0	12.6	14.5	17.5	20.0
20 min	-23.5	10.5	13.8	17.5	19.7
30 min	-26.0	9.8	14.6	16.8	20.2

Table 4.2: Evolution of the temperature distribution, in °C, for the inverted configuration. Since the base was not directly in contact with dry ice, the temperature there was also measured. Measurements stopped after 30 minutes because of the disappearance of the sensitive layer.

t \ y	0 cm	5 cm	10 cm	15 cm	20 cm
5 min	-9.5	17.2	21.9	24.6	50.0
10 min	-20.0	14.0	19.1	23.7	44.0
15 min	-24.9	13.7	20.2	21.0	41.0
20 min	-27.7	10.7	18.0	22.0	37.2
25 min	-46.0	9.6	18.9	22.6	36.5
35 min	-23.4	14.7	22.8	24.8	32.5

Table 4.3: Evolution of the temperature distribution, in °C, for the inverted configuration with hot water on top. The temperature at $y = 20$ cm was directly measured inside the water. The abnormally low temperature measured at $t = 25$ min for $y = 0$ cm may be due to placing the thermocouple too close to the dry ice.

4.3 Magnetic fields

Given the interest, as shown in Sections 3.2 and 3.3, of measuring the momentum of passing particles with a magnetic field, different tests were made with various magnets.

The usage of electromagnets was discarded because a momentum measurement requires the field to be orthogonal to the path of the particles. However, since in diffusion cloud chambers the sensitive layer is always horizontal, any coil would need to be put horizontally. The dimensions of the chamber and the space occupied by the dry ice container made this option hard to develop.

4.3.1 Fields involved

Having to use permanent magnets, a wide magnetic foil placed above the metal plate is an interesting option, not involving the introduction of anything inside the chamber. However, the strongest foil that could be found only reached highly inhomogeneous fields of about 0.07 T. Because of that, passing particles did not show an appreciable deflection distinguishable from vapour currents.

The only option, thus, is to use rare-earth magnets. The opposition of the poles of two horizontally placed neodymium magnets led to a vertical field of about 0.2 T between them. This field could in principle allow to at least estimate the momenta of particles that pass between the magnets.

4.3.2 A problem: condensation

As the quantitative results show, the only way of having a strong, uniform magnetic field inside a region of a diffusion cloud chamber is to use rare-earth magnets. The problem, however, is that putting anything inside the chamber made vapour condense on it. This condensation destroyed the sensitive layer and made tracks impossible to be seen close to the magnets. Because of that, any curvature occurred far from them and might be easily confused with gas motion. The impossibility of turning off the magnetic field made any calibration that could lead to at least semi-quantitative results infeasible.

4.4 Radiation sources

The most accessible particle source for a home-made diffusion cloud chamber is cosmic radiation. The most abundant cosmic particles are, by around 2-3 orders of magnitude, muons. Their vertical flux is about 1 $\text{cm}^{-2}\text{min}^{-1}$, being the angular dependence $\propto \cos^2\theta$, where θ is the zenith angle [11].

Since diffusion cloud chambers are horizontal, the integration of the angular dependence leads to an attenuation in the flux. This attenuation follows a $\sin^3\vartheta$ law, where ϑ is the incident angle measured from the chamber base at which particle paths through the sensitive region are long enough to be seen. Since the surface of the chamber is about 600 cm^2, even $\vartheta \sim 10°$ leads to about an event per minute.

Apart from cosmic ray muons, it might also be possible to observe alpha particles or electrons from background radiation.

4.4.1 Artificial sources

Besides background radiation and cosmic rays, in this project artificial sources of ^{137}Cs and ^{60}Co were also used[1]. Both sources were inside small, flat cases, so they did not remove a significant amount of vapour by condensation.

[1] All the numerical data has been extracted from the ENSDF database [38].

^{137}Cs, which has a half-life of 30.2 years, emits both β^- and γ radiation through two different processes. The main one, with a 95% branching ratio, is a β^- decay to an excited nuclear state of ^{137}Ba followed by a relaxation of this nucleus to its ground state emitting a photon. The mean kinetic energy of the emitted electron is 174 keV, and the energy of the photon 662 keV. There is also a second process, whose branching ratio is 5%, in which ^{137}Cs directly decays to the ground state of ^{137}Ba. This process is a β^- decay, the mean kinetic energy of the electron being 416 keV.

For ^{60}Co, with a half-life of 5.27 years, the decay is almost always, with a branching ratio of 99.9%, to an excited state of ^{60}Ni. This process, a β^- decay, emits an electron with a mean kinetic energy of 96 keV. The decay of ^{60}Ni to its ground state emits two photons with energies 1.173 MeV and 1.332 MeV. The label of the source used indicated that it only emitted γ radiation, so the case was thick enough to stop 96 keV electrons.

Regarding possible safety concerns, both samples were marked as exempt, being the manufacture year 2005. A radiation dosimeter indicated an activity of 6.6 μSv/h and 2.2 μSv/h next to the ^{137}Cs and ^{60}Co sources, respectively. Their activity dropped to 1.7 μSv/h and 1.2 μSv/h when the walls of the chamber were put in between the source and dosimeter. These activities, measured beside the sources, were just one order of magnitude higher than the measured background, 0.2 μSv/h. Because of that, normal manipulation of them should pose no health risk. Furthermore, the European nuclear society places a limit[2] on public exposure to artificial radioactive sources of 1 mSv/year, which is virtually impossible to reach with these sources.

It was also attempted to use a natural radioactive source: an α-emitting uraninite mineral. However, due to the irregularities and size of the mineral, condensation on it removed a lot of vapour and tracks could only be seen for the first few operating seconds.

Anyhow, the uraninite source generated a notable experimental result: tracks of α particles were seen forming towards the mineral. This, apart from proving that tracks are not live pictures of passing particles, also verified the theoretical result that ionisation exponentially increases as a particle loses energy. Because of that, for particles that are stopped by the gas inside the chamber, most ions are created close to the end of the path of the particle.

4.5 Graphical results

A very interesting result that this thesis allowed to obtain is a set of videos showing various nuclear and particle physics phenomena. The entire raw video records can be downloaded from `https://goo.gl/oCBy23`. Apart from that, there are some processes that have been selected and stored into individual videos, downloadable from the ADDI platform:

- *Muon tracks*: they are the most abundant and recognisable events, consisting of thin, visible lines. They are recorded in the files `Muons_1.avi` and `Muons_2.avi`.
- *Alpha particles*: detectable as thick, curved tracks; they are recorded in the files `Alphas_1.avi` and `Alphas_2.avi`.
- *Collisions and scattering*: the observation of two lines that converge into one is probably a sign of a high energy-transfer collision between the incident particle and an electron from the gas. It may as well be a coincidence of three uncorrelated tracks, but this process is very unlikely compared with the observed amount of events. A track with various irregular deflections, on the other hand, can be identified as a multiply-scattered particle.

  A collision between a muon and an electron, stored in `Muon-electron.avi`, a multiple scattering of a particle, stored in `Electron-zigzag.avi`, and a collision between two electrons,

[2] `https://www.euronuclear.org/info/encyclopedia/r/radiation-exposure-dose-limit.htm`

stored in `Electron-electron.avi`, have been selected. This last process could be observed very frequently if the supersaturation and the illumination were good enough.

- *Particle showers*: a remarkable result was that most cosmic rays came in short showers produced by the interaction of incoming particles with the atmosphere. Two showers have been extracted, a horizontal one, recorded in `Horizontal_shower.avi`, and a vertical one, recorded in `Vertical_shower.avi`.

- *Other phenomena*: the ionisation of the medium by the passage of a particle emits low energy electrons that can be identified as short branches that come out of the main track. An event of this kind can be seen in `Secondary_el.avi`.

  Apart from that, when a radiation source was introduced inside the chamber a "web" of particles getting out of the source could be seen. Its various branches indicated the presence of high energy-transfer collisions. An excerpt can be seen in `Web.avi`. Longer excerpts for the used sources can be seen in `Co_60.avi` and `Cs_137.avi`.

  In addition, some tracks seemed to deflect even without any external magnetic field, a deflection that may be attributed to gas currents. An example can be seen in `Bent_no_field.avi`.

- *Currents created by strong magnets*: even though the use of strong rare-earth magnets did not enable a momentum measurement, a distortion of the gas currents was observed close to the poles of the magnets. Since the magnetic field there was almost horizontal, in one of the poles the passing ions were deflected upwards, to a layer with a different velocity distribution, thus creating a vortex. In the other pole, the ions were deflected downwards, to a more static region, creating no visible vortex. The phenomenon can be seen in the file `Magnets.avi`.

Apart from this, longer excerpts can be seen in `Excerpt.avi` and `Excerpt_2.avi`.
Figure 4.4 shows some snapshots of the videos.

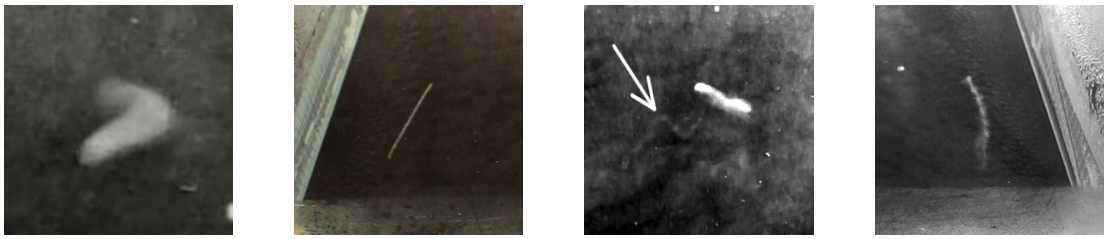

Figure 4.4: Snapshots of some videos. From left to right: an alpha particle, a muon, a high energy-transfer electron-muon collision, and low energy electrons emitted by the ionisation caused by a muon. The third image has been treated to increase the visibility of the event in a static picture.

Chapter 5

Conclusions

This thesis has allowed a systematic theoretical and experimental study of diffusion cloud chambers. These devices are pedagogically highly interesting in nuclear, particle, and condensation physics.

The theoretical analysis quantified the effect of condensation nuclei in cloud formation and led to a discussion of the optimum working conditions in diffusion cloud chambers. That way, pedagogical cloud chambers take advantage of the techniques developed to understand professional devices. What is more, in the early 20^{th} century the main drawback of these works was that they required an extensive use of very specific handbooks and tedious numerical calculations. However, with the advent of information technologies, this is not an inconvenience any more.

The single most significant conclusion drawn out of this study is probably *the importance of a low bottom temperature*. It is this property what guarantees a steady-state distribution with stable track formation. Even though a strong temperature gradient is also required, it has a smaller significance. Furthermore, the study of quantitative models allows to examine the effects that different experimental setups have. In this aspect, the quantitative discussion on the most appropriate alcohol is remarkable. This discussion is hard or even impossible to find in pedagogical papers, and in professional works always assumes that the experimental conditions are completely under control. It may allow as well to develop cloud chambers with more modest cooling systems using different vapours.

Finally, the theoretical insight appeals to many branches of physics, from thermodynamics to fluid dynamics or particle physics. This aspect increases the pedagogical interest of cloud chambers.

The experimental analysis, on the other hand, has induced a precise listing of the building steps and techniques. Knowing *what* should be done and *why* allows an easy arrangement of the experiment that leads to the study of possible improvements. The study also evaluates the experimental problems and requirements that theoretical models miss. *The importance of grazing illumination and of avoiding vapour removal* is here significant.

From a more pedestrian point of view, it is remarkable as well that most of the used material was specifically looked for and acquired for the development of this thesis. With that, the price and accessibility factors, important in pedagogical projects, were taken into account.

Apart from that, a significant amount of graphic material has been produced. These videos visually show events such as particle showers, scattering, radioactivity or magnetic distortion of particle tracks. This material may be useful for the teaching of these subjects.

In conclusion, a more in-depth review than what is usually found in pedagogical papers has been carried out. The usage of modern computation techniques and extensive handbooks, as well as the analysis of different experimental configurations allows an exhaustive study of home-made diffusion cloud chambers. With it, it would be possible to build a permanent chamber for the Faculty, something that because of funding issues has not been done as part of this thesis.

Acknowledgements

I would like to acknowledge many people that have backed the development of this thesis. First of all, I want to thank my supervisors, Gunar Schnell and Charlotte Van Hulse, for their continuous support and advices.

I wish to express my gratitude as well to Íñigo Luis Egusquiza for his constant help, particularly in aspects related to bureaucracy or contact with other research groups in the Faculty. In this aspect, I would like to thank Raúl Montero Santos from the Physical Chemistry Department for lending the glass container for the chamber and the isopropanol, the Mineralogy and Petrology Department, particularly Pedro Pablo Gil and José Francisco Santos, for lending the uraninite sample, Juan Mari Agirregabiria for sharing his magnet collection, and the Microestructural Magnetic and Spectroscopic Characterization of Materials with HIGH-TECH and Biomedical Applications Group, particularly José Javier Saiz Garitaonandia and David Mérida, for their help with radioactive sources and magnetic measurements.

And, in general, I feel grateful to the whole Theoretical Physics and History of Science Department for funding the project and allowing the use of their seminar room to develop it.

Bibliography

[1] C. T. R. Wilson, 'On a Method of Making Visible the Paths of Ionising Particles through a Gas', Proceedings of the Royal Society of London A: Mathematical, Physical and Engineering Sciences **85**, 285–288 (1911).

[2] C. T. R. Wilson, 'Investigations on X-Rays and β-Rays by the Cloud Method. Part I. X-Rays', Proceedings of the Royal Society of London A: Mathematical, Physical and Engineering Sciences **104**, 1–24 (1923).

[3] C. D. Anderson, 'The Positive Electron', Phys. Rev. **43**, 491–494 (1933).

[4] S. H. Neddermeyer and C. D. Anderson, 'Note on the Nature of Cosmic-Ray Particles', Phys. Rev. **51**, 884–886 (1937).

[5] G. D. Rochester and C. Butler, 'Evidence for the Existence of New Unstable Elementary Particles', Nature **160**, 855–857 (1947).

[6] C. T. R. Wilson, 'On a New Type of Expansion Apparatus', Proceedings of the Royal Society of London A: Mathematical, Physical and Engineering Sciences **142**, 88–91 (1933).

[7] L. Hoxton, 'A Continuously Operating Cloud Chamber', Proc. Virginia Acad. Sci. **9**, 23 (1933-34).

[8] R. E. Vollrath, 'A Continuously Active Cloud Chamber', Review of Scientific Instruments **7**, 409–410 (1936).

[9] A. Langsdorf, 'A Continuously Sensitive diffusion Cloud Chamber', Review of Scientific Instruments **10**, 91–103 (1938).

[10] T. S. Needels and C. E. Nielsen, 'A Continuously Sensitive Cloud Chamber', Review of Scientific Instruments **21**, 976–977 (1950).

[11] K. Olive et al., 'Review of Particle Physics', Chin.Phys. **C38**, Chapter 28, 090001 (2014).

[12] P. J. DeMott et al., 'Integrating laboratory and field data to quantify the immersion freezing ice nucleation activity of mineral dust particles', Atmospheric Chemistry and Physics **15**, 393–409 (2015).

[13] R. P. Shutt, E. C. Fowler, D. H. Miller, A. M. Thorndike and W. B. Fowler, 'Π ¯-p Scattering Observed in a Diffusion Cloud Chamber', Phys. Rev. **84**, 1247–1248 (1951).

[14] D. A. Glaser, 'Some Effects of Ionizing Radiation on the Formation of Bubbles in Liquids', Phys. Rev. **87**, 665–665 (1952).

[15] D. R. Lide, ed., *CRC Handbook of Chemistry and Physics*, 90th ed. (CRC Press/Taylor and Francis, 2010).

[16] D. Mackay, W.-Y. Shiu and S. C. L. Kuo-Ching Ma, *Handbook of Physical-Chemical Properties and Environmental Fate for Organic Chemicals*, 2nd ed., Vol. 1 (CRC Press/Taylor and Francis, 2006).

[17] C. L. Yaws, ed., *Transport Properties of Chemicals and Hydrocarbons* (William Andrew Inc., 2009).

[18] W. Thomson, 'LX. On the equilibrium of vapour at a curved surface of liquid', Philosophical Magazine Series 4 **42**, 448–452 (1871).

[19] R. von Helmholtz, 'Untersuchungen über Dämpfe und Nebel, besonders über solche von Lösungen', Annalen der Physik **263**, 508–543 (1886).

[20] P. Tol, 'Technical Note on Colour Schemes', SRON/EPS/TN/09-002, `https://personal.sron.nl/~pault/colourschemes.pdf` Accessed: 17/06/2015 (2012).

[21] J. J. Thomson, *Applications of Dynamics to Physics and Chemistry* (Macmillan and co., London, 1888), p. 165.

[22] N. N. D. Gupta and S. K. Ghosh, 'A Report on the Wilson Cloud Chamber and Its Applications in Physics', Rev. Mod. Phys. **18**, 225–290 (1946).

[23] L. Rayleigh, 'LII. On the theory of surface forces.—III. Effect of slight contaminations', Philosophical Magazine Series 5 **33**, 468–471 (1892).

[24] A. W. Reinold and A. W. Rucker, 'On the Relation between the Thickness and the Surface Tension of Liquid Films', Philosophical Transactions of the Royal Society of London **177**, 627–684 (1886).

[25] A. Langsdorf, 'The Development of a Thermally Activated, Continuously Sensitive Cloud Chamber, and its Use in Nuclear Physics Research', PhD thesis (Massachusetts Institute of Technology, 1937).

[26] J. Wilson, *The Principles of Cloud-Chamber Technique* (Cambridge University Press, 1951).

[27] W. E. Hazen, 'Some Operating Characteristics of the Wilson Cloud Chamber', Review of Scientific Instruments **13**, 247–257 (1942).

[28] R. H. Frost and C. E. Nielsen, 'The Specific Probable Ionization of Electrons Observed with a Wilson Cloud Chamber', Phys. Rev. **91**, 864–870 (1953).

[29] R. S. Carter and W. L. Whittemore, 'The Relative Specific Ionization of Fast Mesons', Phys. Rev. **87**, 494–499 (1952).

[30] K. Olive et al., 'Review of Particle Physics', Chin.Phys. **C38**, Chapter 32, 090001 (2014).

[31] International Commission on Radiation Units and Measurements, ed., *Average Energy Required to Produce an Ion Pair (Report 31)* (ICRU Publications, 1979).

[32] *Atomic and Nuclear Properties of Materials*, Particle Data Group, `http://pdg.lbl.gov/2014/AtomicNuclearProperties/properties8.dat` Accessed: 29/05/2015.

[33] P. Argan, N. D'Angelo and A. Gigli, 'Remarks on the operation of the diffusion cloud chamber (I)', English, Il Nuovo Cimento **1**, 761–784 (1955).

[34] E. A. Mason and S. C. Saxena, 'Approximate Formula for the Thermal Conductivity of Gas Mixtures', Physics of Fluids **1**, 361–369 (1958).

[35] I. Langmuir, 'The Vapor Pressure of Metallic Tungsten', Phys. Rev. **2**, 329–342 (1913).

[36] R. P. Shutt, 'A Theory of Diffusion Cloud Chambers', Review of Scientific Instruments **22**, 730–736 (1951).

[37] S. Tavernier, *Experimental Techniques in Nuclear and Particle Physics*, 1st ed. (Springer-Verlag Berlin Heidelberg, 2010) Chap. 4.

[38] *Evaluated Nuclear Structure Data File*, `http://www.nndc.bnl.gov/ensdf/`, Accessed: 07/06/2015.